ISSN 0915-633X

NATIONAL INSTITUTE FOR FUSION SCIENCE

An Accurate δf Method for Neoclassical Transport Calculation

W.X. Wang, N. Nakajima, S. Murakami
and M. Okamoto

(Received - Feb. 23, 1999)

NIFS-588 Mar. 1999

RESEARCH REPORT
NIFS Series

NAGOYA, JAPAN

An Accurate δf Method for Neoclassical Transport Calculation

W. X. Wang, N. Nakajima, S. Murakami and M. Okamoto
National Institute for Fusion Science, Toki 509-5292, Japan

Abstract

A δf method, solving drift kinetic equation, for neoclassical transport calculation is presented in detail. It is demonstrated that valid results essentially rely on the correct evaluation of marker density g in weight calculation. A general and accurate weighting scheme is developed without using some assumed g in weight equation for advancing particle weights, unlike the previous schemes. This scheme employs an additional weight function to directly solve g from its kinetic equation using the idea of δf method. Therefore the severe constraint that the real marker distribution must be consistent with the initially assumed g during a simulation is relaxed. An improved like-particle collision scheme is presented. By performing compensation for momentum, energy and particle losses arising from numerical errors, the conservations of all the three quantities are greatly improved during collisions. Ion neoclassical transport due to self-collisions is examined under finite banana case as well as zero banana limit. A solution with zero particle and zero energy flux (in case of no temperature gradient) over whole poloidal section is obtained. With the improvement in both like-particle collision scheme and weighting scheme, the δf simulation shows a significantly upgraded performance for neoclassical transport study.

Keywords: neoclassical transport, drift kinetic equation, δf algorithm, Monte Carlo collision operator

I. INTRODUCTION

The δf particle simulation[1-5] has been widely used to study the kinetic phenomena in plasmas. In this method, the particle distribution function f is divided into an equilibrium distribution f_0 plus a perturbation δf (or f_1 used in this paper); the f_0 is assumed to be known analytically and only perturbed δf is solved from the the dynamics of a finite number of particles. Compared to conventional full-f method the noise level is reduced by a factor of $(\delta f/f_0)^2$ in the δf method because numerical noise associated with the representation of f_0 is completely removed[1,5]. In the other words much less simulation particles are required to achieve the same accuracy as in full-f simulation. An important character of δf method is that simulation particles are assigned weights which evolve in time so as to effectively model the source terms in the equation of δf. Thus in δf method the particle dynamics includes, in addition to the motion in $\vec{x}$-$\vec{v}$ phase space, the evolution of weights.

The δf method was initially proposed for nondiffusive most Hamiltonian particle motion[1,2]. Recent years it has been applied to study neoclassical transport phenomena in fusion plasmas[6,7]. The study of neoclassical transport phenomena is newly motivated by recent development in fusion experiments where plasmas are operated in parameter regimes beyond the valid scope of the conventional neoclassical theory[8]. For example, in H-mode edge plasma and reversed shear core plasma the essential assumptions for the neoclassical theory, namely $\rho_p \ll L_r$ and $M_p \ll 1$, are no longer valid, where ρ_p is poloidal Larmor radius, L_r is the radial gradient length of plasma parameters, and M_p is poloidal Mach number. The modifications to the neoclassical theory are required for taking into account finite banana width dynamics, strong radial electric field with large radial gradient and non-standard orbit topology near magnetic axis. The δf particle simulation, solving drift kinetic equation, can be a powerful tool for neoclassical transport calculation[6]. In addition to low noise, another merit of using δf method for neoclassical transport calculation is no profile relaxation effects which are troublesome in full-f simulations. The thermodynamic "forces" such as temperature gradient ∇T and pressure gradient ∇p driving plasma transport are controllable.

Accurate implementation of Coulomb collisions is an important ingredient for neoclassical transport calculation. Accuracy of different approximate Fokker-Planck operators directly influences simulation results of fluxes as well as other neoclassical transport quantities. For example, unphysical particle flux could be created by like-particle collisions alone if we fail to maintain the momentum conservation in the collision calculation. It has been a long effort to develop accurate and effective collision operators for plasma simulations. As discussed in previous works[6,9], collisions between ions and electrons usually can simply be modeled by employing the large mass ratio approximation. The first purpose of this paper is to present a linear like-particle collision scheme, accurately conserving the particle number, momentum and energy, for neoclassical transport calculation using the δf method. Our collision scheme is developed from the collision model introduced by Catto and Tsang[10], as well as Xu and Rosenbluth[11], and then implemented and modified by Dimits and Cohen[9], and Lin, Tang and Lee[6]. By introducing the restoring terms to compensate momentum, energy and particle losses due to numerical errors, all three quantities are conserved near perfectly. The benchmark calculation of neoclassical transport using the present collision scheme demonstrates the increased accuracy in results. The use of a linear collision operator is consistent with the δf methods which solve linearized kinetic equations, and the present collision scheme seems to be most adequate for δf simulations.

The calculation of particle weight is crucial in a δf simulation. The second purpose of this paper is

to present a general and accurate weighting scheme for solving the drift kinetic equation with the drift term retained. In the previous δf simulations[6,7] of neoclassical transport, the drift kinetic equation was solved using the so called nonlinear weighting scheme[4] in which the distribution function f is used to replace the marker (i.e, simulation particle) density g in weight equation. This nonlinear weighting scheme was initially derived for nonlinear gyrokinetic equation with nondiffusive motion, and in fact it cannot be directly extended to the drift kinetic equation with diffusive motion due to Coulomb collision processes. Recently, Chen and White[12] have given a rigorous derivation of collisional δf algorithm by treating the weight as a new dimension of particle motion. Their derivation is able to elucidate the feature and unconventional role of the marker density g. However. the question how to evaluate g for weight calculation still remains to be solved. We show the importance of estimating g in δf method for neoclassical transport calculation. In a δf particle simulation. markers may diffuse through and loss from the simulation domain because of radial drift and collisional processes. Then it is necessary to add new markers during the simulation so as to maintain sufficient particles (well populated phase space). A natural problem therefore arises. that is how to add new markers and what determines the way for new markers to be added. This problem is closely related to the weight calculation. We demonstrate that the nonlinear weighting scheme is ineffective or inaccurate for solving the drift kinetic equation because of a severe constraint that the relation $g = f$ must be hold accurately in a simulation. Otherwise, correct results can not be guaranteed. Generally. it is difficult even impossible to get rid of this restriction. Here, we directly evaluate g from its kinetic equation using the idea of δf method. The resultant weighting scheme consists of two weight equations. and is more effective and accurate to solve the drift kinetic equation.

The paper is organized as follows. In Sec. II we formulate the δf algorithm for solving drift kinetic equation using the approach adopted by Chen and White. In Sec. III we present a like-particle collision scheme for δf simulation. The essentials in weight calculation and the difficulty in applying the nonlinear weighting scheme to solve the drift kinetic equation are demonstrated and discussed in Sec. IV. These results motivate us to develop a more effective and more accurate weighting scheme which is presented in Sec. V. The main results of the paper are summarized in Sec. VI.

II. δf FORMALISM OF DRIFT KINETIC EQUATION

Let us start from the well-known drift kinetic equation[8] for a guiding center distribution function $f(\vec{v},\vec{x})$ in phase space $\{\vec{v},\vec{x}\}$,

$$\frac{\partial f}{\partial t} + (\vec{v_\parallel} + \vec{v_d}) \cdot \nabla f = C(f,f). \tag{1}$$

where $\vec{v_d}$ is the guiding center velocity and C is the Coulomb collision operator. Separating f into two parts $f = f_0 + f_1$, we rewrite the drift kinetic equation as

$$\frac{\partial f_0}{\partial t} + \vec{v_\parallel} \cdot \nabla f_0 - C(f_0, f_0) = 0 \tag{2}$$

and

$$\frac{\partial f_1}{\partial t} + (\vec{v_\parallel} + \vec{v_d}) \cdot \nabla f_1 - C(f_1, f_0) = -\vec{v_d} \cdot \nabla f_0 + C(f_0, f_1) + C(f_1, f_1). \tag{3}$$

Note that Eqs. (2) and (3) are completely equivalent to Eq.(1). A steady state solution to Eq.(2) is a Maxwellian distribution, $f_0 = f_M$. If $f_1 \ll f_0$ holds, based on expansion in a small parameter (which depends on situation under consideration). the nonlinear part of collision operator in Eq.(3) may be neglected to obtain

$$\frac{\partial f_1}{\partial t} + (\vec{v_\parallel} + \vec{v_d}) \cdot \nabla f_1 - C(f_1, f_0) = -\vec{v_d} \cdot \nabla f_0 + C(f_0, f_1). \tag{4}$$

Since the drift term is retained, this equation can take into account the finite banana width effect which may become substantial in present tokamak operation. If the banana width Δ_b is negligible compared with the radial gradient length of plasma parameters, Eq.(3) can be further simplified to the form very familiar to us

$$\frac{\partial f_1}{\partial t}+\vec{v_\parallel}\cdot\nabla f_1-C(f_1,f_0)=-\vec{v_d}\cdot\nabla f_0+C(f_0,f_1). \quad (5)$$

This equation provides the starting point for conventional neoclassical transport analysis[8]. Now we consider to solve linearized equations (4) and (5) utilizing particle simulation techniques. From the technical view point of particle simulation, the δf method differs from the full-f method only by an evolving simulation particle weight which is introduced to effectively treat the "source" terms at the right hand sides of Eqs. (4) and (5). The conventionally used definition for the particle weight is

$$w = f_1/g, \quad (6)$$

where g is the numerically evolved simulation particle distribution[4,5]. This definition works well for nondiffusive most Hamiltonian particle motion, but causes difficulty in deriving the weight equation when particle motion is diffusive due to, for example, Coulomb collisions[12]. Here. we adopt the approach proposed by Chen and White[12] to derive the weight equation. The weight is treated as a new dimension of the particle motion, in addition to the usual dimensions of $(\vec{x},\vec{v})$ phase space. The simulation particles are described by a marker distribution function, $F_M(\vec{x},\vec{v},w,t)$, in the extended phase space $(\vec{x},\vec{v},w)$. The marker distribution function F_M, according to the equivalence between Langevian equations and the Fokker-Planck equation, obeys the following kinetic equation:

$$\frac{D}{Dt}F_M+\frac{\partial}{\partial w}(\dot{w}F_M)=S_M(\vec{x},\vec{v},w,t), \quad (7)$$

where the notation $D/Dt(f)$ denotes, for an arbitrary f.

$$\frac{D}{Dt}f=\frac{\partial f}{\partial t}+(\vec{v_\parallel}+\vec{v_d})\cdot\nabla f-C(f,f_0) \quad (8)$$

or

$$\frac{D}{Dt}f=\frac{\partial f}{\partial t}+\vec{v_\parallel}\cdot\nabla f-C(f,f_0), \quad (9)$$

corresponding to Eq.(4) or (5), respectively. Since markers may diffuse through and loss from the simulation domain, a source S_M for markers is introduced to provide, in addition to the initial loading, further control of the marker population. Each marker is pushed in the extended phase space along the characteristics

$$\frac{d\vec{x}}{dt}=\dot{\vec{x}}, \quad \frac{d\vec{v}}{dt}=\dot{\vec{v}}, \quad \text{and} \quad \frac{dw}{dt}=\dot{w}. \quad (10)$$

The numerical representation of F_M is

$$F_M(\vec{x},\vec{v},w,t)=\sum_j \delta(\vec{x}-\vec{x}_j(t))\delta(\vec{v}-\vec{v}_j(t))\delta(w-w_j(t)). \quad (11)$$

Set that f_1 and F_M have the following relation

$$f_1(\vec{x},\vec{v},t)=\int wF_M dw. \quad (12)$$

Then f_1 is numerically represented as

$$f_1(\vec{x},\vec{v},t)=\sum_j w_j\delta(\vec{x}-\vec{x}_j(t))\delta(\vec{v}-\vec{v}_j(t)). \quad (13)$$

The weight equation is determined by requiring that Eqs. (4) or (5), (7) and (12) are consistent with each other. Comparing the resultant equation of $\int w\times$Eq.(7)dw to Eq. (4) or (5), the weight equation is determined as

$$\dot{w}=\frac{1}{g}\left[-\int wS_M dw-\vec{v_d}\cdot\nabla f_0+C(f_0,f_1)\right], \quad (14)$$

where

$$g(\vec{x},\vec{v},t)\equiv\int F_M(\vec{x},\vec{v},w,t)dw \quad (15)$$

is the integrated marker distribution function in the original phase space and satisfies the following equation

$$\frac{D}{Dt}g=\int S_M dw. \quad (16)$$

Equation (14), along with the equations of motion in original phase space, represents the basic formalism for the δf method, and Eq. (14) is the governing equation for the δf method.

III. LIKE-PARTICLE COLLISION SCHEME

The linearized like-particle collision operator is written as

$$C^l(f_1) = C(f_1, f_0) + C(f_0, f_1). \quad (17)$$

The first term on the right-hand side, referred to $C_{TP}(f_1)$ hereafter, is drag and diffusion part which describes the test particle (represented by f_1) collisions with Maxwellian field particles (represented by f_0). In a drift kinetic simulation the test particle operator can be implemented by utilizing standard Monte Carlo technique[9 11 13]. The second term on the right-hand side of Eq.(17) accounts for the perturbation of the field particle. This term is complicated in form and is not sensitive to the details of f_1. Therefore instead of using such a complicated form, it is convenient to replace it with a simpler equation as follows[10 11]

$$C(f_0, f_1) = P(\vec{x}, \vec{v}) f_M \quad (18)$$

where P is determined from the constraint of momentum and energy conservation. The momentum and energy removed by the first term in Eq.(17) is replenished in a Maxwellian distribution. A possible expression for P is determined as[10 11]

$$P(\vec{x}, \vec{v}) = -\vec{v} \cdot \vec{p} - (\frac{v^2}{v_{th}^2} - \frac{3}{2})E. \quad (19)$$

where

$$\vec{p}(\vec{x}) \equiv \frac{2}{n v_{th}^2} \int \vec{v} C_{TP} d\vec{v} = \frac{2}{v_{th}^2} \frac{d}{dt} \langle \vec{v} \rangle_{TP}. \quad (20)$$

$$E(\vec{x}) \equiv \frac{2}{3 n v_{th}^2} \int v^2 C_{TP} d\vec{v} = \frac{2}{3 v_{th}^2} \frac{d}{dt} \langle v^2 \rangle_{TP}. \quad (21)$$

Here n and v_{th} denote the particle density and thermal velocity, respectively. To make the physical meaning clear at a glance, we use notations $\frac{d}{dt}\langle \vec{v} \rangle_{TP}$ and $\frac{d}{dt}\langle v^2 \rangle_{TP}$ to denote the averaged change of particle velocity and energy due to the test particle collisions (in later descriptions, similar notations will be used without further explanation).

The momentum and energy conservation term Pf_M appears as a source term in the linearized equations. Dimits and Cohen[9] implemented this term using weight method in δf particle simulation. For like-particle collisions, the collision operator should annihilate a shifted Maxwellian. Lin, Tang and Lee[6] found that like-particle collisions implemented using Eq.(19) fail to maintain a shifted Maxwellian since the velocity dependence of the momentum and energy loss rates due to test-particle collisions is not taken into account. By calculating the momentum and energy loss rates with correct velocity dependence, they modified the conservation term to

$$\begin{aligned} P(\vec{x}, \vec{v}) &= -3\sqrt{\frac{\pi}{2}} \phi(y) (\frac{v_{th}}{v})^3 \vec{v} \cdot \vec{p} \\ &\quad -3\sqrt{\frac{\pi}{2}} \left[\phi(y) - \frac{d\phi}{dy} \right] \frac{v_{th}}{v} E \\ &= \vec{A} \cdot \frac{d}{dt} \langle \vec{v} \rangle_{TP} + B \frac{d}{dt} \langle v^2 \rangle_{TP}. \end{aligned} \quad (22)$$

where $\phi(y)$ is the Maxwellian integral defined by

$$\phi(y) = \frac{2}{\sqrt{\pi}} \int_0^y e^{-t} \sqrt{t} dt$$

with $y = v^2/v_{th}^2$, and the notations $\vec{A}$ and B are used for the convenience of description.

Theoretically the operator represented by Eqs.(17), (18) and (22) exactly satisfies all of conservation laws, i.e. particle number, momentum and energy conservation as follows,

$$\int (C_{TP} + P f_M) d\vec{v} = 0, \quad (23)$$

$$\int \vec{v} (C_{TP} + P f_M) d\vec{v} = 0. \quad (24)$$

$$\int v^2 (C_{TP} + P f_M) d\vec{v} = 0. \quad (25)$$

Numerically, in implementation of Eqs.(17), (18) and (22) in a δf simulation the accuracy in particle, momentum and energy conservation is not sufficient. As will be demonstrated by simulation examples in this section, there are still considerable non-vanishing numerical errors in $\frac{d}{dt}\langle \vec{v} \rangle_{TP+P}$, $\frac{d}{dt}\langle v^2 \rangle_{TP+P}$ and $\frac{d}{dt}\langle v^0 \rangle_P$ (note that $\frac{d}{dt}\langle v^0 \rangle_{TP} = 0$ since the implementation of C_{TP} does not change particle weight).

and the numerical errors may get so enlarged as to influence the results of a neoclassical transport calculation. The idea called to our mind first is to introduce additional term to restore momentum and energy conservation directly as follows,

$$P_1 f_M = \left(\vec{A} \cdot \frac{d}{dt} \langle \vec{v} \rangle_{TP+P} + B \frac{d}{dt} \langle v^2 \rangle_{TP+P} \right) f_M. \tag{26}$$

Then we have, theoretically,

$$\begin{aligned} \int \vec{v}(C_{TP} + P f_M + P_1 f_M) d\vec{v} &= 0 \text{ and} \\ \int v^2 (C_{TP} + P f_M + P_1 f_M) d\vec{v} &= 0, \end{aligned}$$

even though there are non-vanishing $\frac{d}{dt}\langle \vec{v} \rangle_{TP+P}$ and $\frac{d}{dt}\langle v^2 \rangle_{TP+P}$. The term $P_1 f_M$ works to compensate the momentum and energy loss, $\frac{d}{dt}\langle \vec{v} \rangle_{TP+P}$ and $\frac{d}{dt}\langle v^2 \rangle_{TP+P}$, just as $P f_M$ works to compensate the momentum and energy loss, $\frac{d}{dt}\langle \vec{v} \rangle_{TP}$ and $\frac{d}{dt}\langle v^2 \rangle_{TP}$. Of course, the property of particle conservation should not be changed by the introducing $P_1 f_M$. Theoretically this point is assured by

$$\int P_1 f_M d\vec{v} = 0.$$

Working along this line, we can repeat this procedure if necessary. For example, we can introduce the term

$$\begin{aligned} P_2 f_M &= \left(\vec{A} \cdot \frac{d}{dt} \langle \vec{v} \rangle_{TP+P+P_1} \right. \\ &\quad \left. + B \frac{d}{dt} \langle v^2 \rangle_{TP+P+P_1} \right) f_M \end{aligned} \tag{27}$$

to compensate the momentum and energy losses due to $C_{TP} + P f_M + P_1 f_M$, and so on.

To test and compare the accuracy of like-particle collision schemes, we solve, only in velocity space, following equation

$$\frac{\partial f}{\partial t} = C^l(f) \tag{28}$$

with initial distribution function being a shifted Maxwellian. 4000 particles are used in our test. The changes of total energy, total momentum and total weight (particle number) are shown in Fig. 1. The curve with open circles represents the result using the previous scheme of Lin et.al.[6]. Figure 1(a) shows that the deviation of the energy from the initial value is largely reduced as $P_1 f_M$ [Eq.(26)] is implemented (represented by the curve with squares). The further reduction in the energy deviation is obtained when $P_2 f_M$ [Eq.(27)] is added (represented by the curve with triangles). This can be seen more clearly from Fig. 1(b) being enlarged from Fig. 1(a). Figure 1(c) shows that the restoring terms $P_1 f_M$ and $P_2 f_M$ do not work for the improvement of momentum conservation as effectively as they do for energy. As $P_1 f_M$ is implemented, the deviation of momentum from the initial value still remains at a significant level (represented by the curve with squares) even though it is considerably reduced from the result without $P_1 f_M$. Moreover, the further reduction is not obtained when $P_2 f_M$ is added (represented by the curve with triangles). Now let us see the particle number conservation behavior presented in Fig. 1(d). For the previous collision scheme, the particle number conservation property is the best among its three conservation laws. The particle number is conserved within the accuracy of 10% for this example. [see the curve with open circles in Fig. 1(d)]. The introduction of the momentum and energy restoring terms $P_1 f_M$ and $P_2 f_M$ makes particle conservation worse. From Figs. 1(c) and 1(d), it is observed that the evolving histories of momentum deviation and particle number deviation are very similar when $P_1 f_M$ and $P_2 f_M$ are introduced. This observation indicates that the momentum conservation property is closely related to the particle conservation property. The above fact reminds us that the momentum conservation could be improved if we can find the way to improve the particle conservation. Based on this consideration, we introduce additional terms as follows to restore particle conservation just as we have done for momentum and energy conservation

$$Q_1 f_M = D(\vec{x}, \vec{v}) f_M \frac{d}{dt} \langle v^0 \rangle_P, \tag{29}$$

$$Q_2 f_M = D(\vec{x}, \vec{v}) f_M \frac{d}{dt}\langle v^0 \rangle_{P+P_1+Q_1}. \qquad (30)$$

.

.

.

The $Q_1 f_M$ and $Q_2 f_M$ work to compensate the numerical particle losses $\frac{d}{dt}\langle v^0 \rangle_P$ and $\frac{d}{dt}\langle v^0 \rangle_{P+P_1+Q_1}$, respectively. The function $D(\vec{x}, \vec{v})$ satisfies

$$\begin{aligned} \frac{1}{n}\int D(\vec{x}, \vec{v}) f_M d\vec{v} &= -1, \\ \int \vec{v} D(\vec{x}, \vec{v}) f_M d\vec{v} &= 0, \\ \int v^2 D(\vec{x}, \vec{v}) f_M d\vec{v} &= 0. \end{aligned} \qquad (31)$$

Equation (31) states that $Q_1 f_M$ and $Q_2 f_M$ work only to restore particle conservation but do not change the momentum and energy conservation property. The D determined from Eq. (31) is not unique. Here we take

$$D(\vec{x}, \vec{v}) = 3\sqrt{\frac{\pi}{2}}\left[\phi(y) - \frac{d\phi}{dy}\right]\frac{v_{th}}{v} - 1. \qquad (32)$$

Note that since $Q_1 f_M$ is newly added, Eq. (27) should be modified to

$$\begin{aligned} P_2 f_M \quad = \quad & \left(\vec{A}\cdot\frac{d}{dt}\langle \vec{v} \rangle_{TP+P+P_1+Q_1} \right. \\ & \left. + B\frac{d}{dt}\langle v^2 \rangle_{TP+P+P_1+Q_1}\right) f_M. \end{aligned} \qquad (33)$$

where $\frac{d}{dt}\langle \vec{v} \rangle_{TP+P+P_1+Q_1}$ and $\frac{d}{dt}\langle v^2 \rangle_{TP+P+P_1+Q_1}$ are momentum and energy losses due to $C_{TP} + Pf_M + P_1 f_M + Q_1 f_M$, respectively. The results with particle restoring term $Q_1 f_M$ and $Q_2 f_M$ implemented are indicated by the curves with solid circles in Fig. 1. It is found that the particle conservation is greatly improved. Correspondingly, the momentum conservation is greatly improved; while the excellent accuracy in energy conservation still remains. Equations (26), (33), (29) and (30) along with Eqs. (17), (18) and (22) represent an improved collision scheme.

In order to verify that the improved collision scheme works well for neoclassical transport calculation, we next solve Eq. (5) for ions including only ion-ion collisions, using the δf method. We employ a simple toroidal equilibrium described by magnetic field model

$$\vec{B} = \frac{B_0}{1+\epsilon\cos\theta}\left[\hat{o} + \frac{\epsilon}{q(r)}\hat{\theta}\right]. \qquad (34)$$

where r, θ and o are the toroidal coordinates. B_0 is B on axis, ϵ and q are the inverse aspect ratio and safety factor, respectively. In special case of zero ion temperature gradient $\nabla T_i = 0$, Eq. (5) has an exact steady-state solution of shifted Maxwellian[8],

$$f_{i1} = \frac{2v_\parallel u_{\parallel T}}{v_{thi}^2} f_{i0} \qquad (35)$$

with the parallel velocity given by

$$u_{\parallel T} = -\frac{q}{\epsilon}\frac{v_{thi}^2}{2\Omega_i}\left(\frac{d\ln n_i}{dr} + \frac{e}{T}\frac{d\Phi}{dr}\right), \qquad (36)$$

where Ω_i is ion gyrofrequency, e is ion charge and Φ is the radial electric potential. Since the drift velocity v_d is even in $v_\parallel$, this solution gives no particle flux and energy flux. The results of simulations carried out with $\nabla n_i \neq 0$, $\nabla T_i = 0$ and $\nabla\Phi = 0$ are presented in Fig. 2. When the improved collision scheme is used, the particle flux [Fig. 2(a)] and energy flux [Fig. 2(b)] indeed drop to zero at steady state and the parallel velocity [Fig. 2(c)] is in good agreement with the theory; while the simulation using the previous scheme still gives definite positive particle and energy fluxes and a smaller parallel velocity in steady state. The feature behind this difference between applying the two collision schemes becomes clearly evident if we see the distribution function f_1 in steady-state [Fig. 2(d)]. The simulation using the improved collision scheme can well reproduce the shifted Maxwellian which is anti-symmetric about $v_\parallel = 0$. The solution using the previous scheme fails to do so. Thus the non-vanishing particle and energy fluxes and smaller $u_\parallel$ arise from the fact that the anti-symmetry is distorted.

It should be pointed out that the compensation terms, $P_1 f_M$, $Q_1 f_M$, $P_2 f_M$ and $Q_2 f_M$, introduce no additional effective collisions. This can be understood from the following discussions. It should be

observed that these newly introduced compensation terms would be zero (or would not work) if Pf_M could accurately restore momentum and energy conservations. We know that a simpler Pf_M is used for the replacement of $C(f_M, f_1)$, and that only from the requirement of the three conservation laws, the function P can not be uniquely determined. Both Pf_M and $(P+P_1+Q_1+P_2+Q_2)f_M$ can be viewed as an approximation to $C(f_M, f_1)$. Theoretically, it is difficult to verify which one is more reasonable. However, the results of tests show that the present collision scheme does a much better performance.

IV. CALCULATION OF PARTICLE WEIGHT

The calculation of particle weight takes a central position in a δf simulation. The weight is calculated by Eq. (14). The critical point of implementing Eq. (14) is how to evaluate the distribution function $g(\vec{x}, \vec{v}, t)$.

In principle one may numerically evaluate g from F_M using Eq. (15). However, it should be noted that the evaluated g could be very noisy. Moreover, since g appears in the denominator of weight equation (14), numerical difficulties may arise for particles at the tail of the distribution where g is small and most noisy. Therefore, as pointed out by Chen and White[12], numerical evaluation of g should be avoided whenever possible. Indeed, so far in the application of the δf method the numerical evaluation of g has been avoided by loading the markers according to a known explicit solution of the kinetic equations[9,11], or by using the fact that in nondiffusive motion g can be advanced along the particle trajectory[5]. Usually it is difficult to use these methods for δf simulation of neoclassical transport where particle motion is diffusive. Chen and White also give a general discussion for evaluating g. Further discussion will be given next with respect to solving Eq. (4) and Eq. (5) by δf method.

Equation (5) can be solved on a single magnetic surface since the drift motion is neglected. Markers (simulations particles) move along the zeroth-order orbit subject to test particle collisions and are bound on the magnetic surface where they are initially loaded. Since no marker is lost from the surface, it is not necessary to add new markers. i.e, we can take the source $S_M = 0$. In this case the solution of Eq. (16) for g corresponding to Eq. (5) is $g = f_M$. Thus, there is no special difficulty in solving the drift kinetic equation without the drift term. The situation is quite different in solving Eq. (4) where the drift term is retained in order to include the important finite banana width dynamics of ion neoclassical transport. In this case, the motion of markers is no longer bound on a single magnetic surface due to radial drift, and a simulation domain extending in radial direction is required to solve the equation. Because of collision processes (with no momentum and energy conservations) markers will diffuse through and loss from the simulation domain. To control that the phase space is well populated, we need to add new markers via a source S_M. Noting that now the kinetic equation of g, Eq. (16), is similar to the kinetic equation of f, one may load particles with the equilibrium distribution $F_M(t=0) = f_0\delta(w)$ (i.e, $g(t=0) = f_0$) and then use $g \approx f = f_0 + f_1$, leading to $g_j \approx f_{0j}/(1-w_j)$ for a particle j, in Eq. (14) for advancing particle weight. This is so called the nonlinear weighting scheme which was initially proposed by Parker and Lee[4] to solve nonlinear gyrokinetic equation with nondiffusive motion, and has been used in the gyrokinetic particle simulation of neoclassical transport[6,7]. It should be pointed out that much caution must be paid when this nonlinear weighting scheme is applied to solve the drift kinetic equation (4). It must be made sure that the approximation $g \approx f$ is correctly represented by marker distribution. If we fail to do so, the correct result

cannot be expected. It should be noted that the relation $g = f$ is not automatically or simply satisfied during a simulation because the equations governing g (Eq.16) and f (Eq.1) are different. In some simple case, the requirement $g = f$, in principle, could be achieved by choosing an appropriate marker source S_M.

In order to demonstrate the essence of estimating g for δf method, we now solve Eq. (4) for ions including only ion-ion collisions using the nonlinear weighting scheme. Again, we employ the simple analytic equilibrium, Eq. (34), and zeroth-order distribution with linear density profile but no temperature gradient ($\nabla T = 0$). Simulation domain is taken as the whole poloidal section extending from $r = 0$ to boundary $r = a$ with a the minor radius of the tours. Unlike the case of Eq. (5), to solve Eq. (4) we need boundary conditions. Boundaries should be treated in a manner consistent with the physical boundaries. Here particles are considered to be lost from the boundary $r = a$; markers hitting this boundary are removed from simulations. Two simulations are performed with different marker sources referred to A and B. As is shown in Fig. 3, the use of different sources results in different marker distribution function g, and the simulation results of particle and energy fluxes sensitively depend on whether the approximation $g \approx f$ is correctly represented by marker distribution. We can examine how far g approximates f by comparing g with f_0 recognizing that $f_1 \ll f_0$. The density profiles of markers at several time points of steady state are shown in Fig. 3(a). The density profile resulting from the use of $S_{M\,A}$ deviates far from that of f_0 (i.e. initial density profile). This result indicates that g does not approximate f. When an appropriate $S_{M\,B}$ is used to add new markers, the density profile is maintained to be close to that of f_0, which indicates that $g \approx f$ is implemented in this simulation. As $g \approx f$ is implemented in the simulation, the both particle flux and energy flux evolve to vanish in steady state, as shown in Figs. 3(b) and 3(c), owing to the momentum and energy conservation of like particle collisions and $\nabla T = 0$. The particle and energy flux at different radial positions are plotted in Figs. 3(d) and 3(e). The simulation with $g \approx f$ well implemented leads to the fluxes to vanish at whole region of poloidal section except the boundary where particle losses result in large particle and energy flux. When we fail to implement $g \approx f$, using the source $S_{M\,A}$, the simulation leads to particle and energy flux which are obviously unphysical. The particle and energy flux, resulting from using the non-conservation operator C_{TP} are also plotted. The time evolution of parallel velocity at $r/a = 0.5$ is shown in Fig. 3(f). It is interesting to see that parallel velocity is slightly reduced as the finite banana width dynamics are included. The radial profile of parallel velocity is shown in Fig. 3(g).

We have demonstrated that distribution function g assumed in Eq. (14) for weight calculation must be consistent with the marker distribution of Eq. (15). If we ignore or fail to fulfill this condition in a simulation, correct results cannot be guaranteed. For some simple case like the above example with only linear density profile but no temperature gradient, we may realize this situation via the choice of an appropriate source S_M. However for complicated practical simulation including, for example, both density and temperature gradient, it is difficult even impossible to find an appropriate S_M; Moreover, for the nonlinear weighting scheme where g is assumed to be f in Eq. (14), exactly saying, we cannot confirm whether $g = f$ is correctly implemented since f is unknown. Therefore for practical application an effective and more accurate weighting scheme is required. We now present such a weighting scheme in the next section.

V. GENERAL AND ACCURATE WEIGHTING SCHEME

Instead of using $g = f$ in Eq. (14) for advancing particle weights, we now consider to solve g from Eq. (16) with $g(t=0) = f_0$ (corresponding to a loading $F_M(t=0) = f_0\delta(w)$). Setting $g = g_0 + g_1$, we separate exactly Eq. (16) into following two equations,

$$\frac{\partial g_0}{\partial t} + \vec{v_\parallel} \cdot \nabla g_0 - C(g_0, f_0) = 0, \tag{37}$$

$$\frac{\partial g_1}{\partial t} + (\vec{v_\parallel} + \vec{v_d}) \cdot \nabla g_1 - C(g_1, f_0) = -\vec{v_d} \cdot \nabla g_0 + \int S_M dw, \tag{38}$$

with the solution of Eq. (37) being $g_0 = f_0 = f_M$ and initial condition of Eq. (38) being $g_1(t=0) = 0$. We now solve Eq. (38) using the idea of δf method. To this end, we introduce a weight ω and a marker distribution function $G_M(\vec{x}, \vec{v}, \omega, t)$ in extended phase space $(\vec{x}, \vec{v}, \omega)$. Let G_M obey the kinetic equation

$$\frac{D}{Dt} G_M + \frac{\partial}{\partial \omega}(\dot{\omega} G_M) = \Omega_M(\vec{x}, \vec{v}, \omega, t) \tag{39}$$

with initial condition $G_M(t=0) = f_0\delta(\omega)$, and relate to g_1 through the following relation

$$g_1(\vec{x}, \vec{v}, t) = \int \omega G_M d\omega. \tag{40}$$

Here a source term Ω_M, like S_M in Eq. (7), is introduced to control the marker population. From the requirement that Eqs. (38), (39) and (40) are consistent with each other, the equation for weight ω is determined as

$$\dot{\omega} = \frac{1}{h}\left[-\int \omega \Omega_M d\omega - \vec{v_d} \cdot \nabla f_0 + \int S_M dw \right], \tag{41}$$

where the distribution function $h(\vec{x}, \vec{v}, t)$ is defined by

$$h \equiv \int G_M(\vec{x}, \vec{v}, \omega, t) d\omega, \tag{42}$$

and satisfies

$$\frac{D}{Dt} h = \int \Omega_M d\omega. \tag{43}$$

Taking

$$\int \Omega_M d\omega = \int S_M dw, \tag{44}$$

then Eq. (43) and Eq. (16) become the same, and we have

$$h(\vec{x}, \vec{v}, t) = g(\vec{x}, \vec{v}, t). \tag{45}$$

For a simulation particle of index j, we have

$$g_j = g_{0j} + \omega_j h_j \tag{46}$$

which gives

$$g_j = \frac{1}{1 - \omega_j} f_{0j}. \tag{47}$$

Substituting Eq. (46) into Eqs.(14) and (41), we obtain the accurate weight equations for a marker as follows

$$\dot{w} = \frac{1 - \omega}{f_0}\left[-\int w S_M dw - \vec{v_d} \cdot \nabla f_0 + C(f_0, f_1) \right], \tag{48}$$

$$\dot{\omega} = \frac{1 - \omega}{f_0}\left[-\int \omega \Omega_M d\omega - \vec{v_d} \cdot \nabla f_0 + \int S_M dw \right]. \tag{49}$$

Now each simulation particle is assigned two weights rather than one, and the second weight ω is introduced to evaluate g (exactly saying, g_1) effectively. The motion of markers in original phase space is independent of weights and this suggests us to solve Eq. (4) and Eq. (38) simultaneously using only one set of markers. Equations (48) and (49) represent a general and accurate weighting scheme. The new scheme elucidates the close relationship between the weight calculation and the way of adding new markers. All answers to the question presented in the Introduction concerning the addition of new markers can be found from these two equations.

Let us see the relation of this accurate weighting scheme to the previous nonlinear weighting scheme. If we choose S_M and Ω_M such that $S_M = S(\vec{r}, \vec{v}, t)\delta(w)$, $\Omega_M = S(\vec{r}, \vec{v}, t)\delta(\omega)$ and

$$\int S_M dw = C(f_0, f_1),$$

then Eqs.(48) and (49) are identical and reduce to the nonlinear weighting scheme

$$\dot{w} = \frac{1 - w}{f_0}\left[-\vec{v_d} \cdot \nabla f_0 + C(f_0, f_1) \right]. \tag{50}$$

(In this case, the equations for g and f become identical.) However this choice is practically infeasible. It makes the problem returning back to its original point. The marker source so chosen is not implementable in the $\vec{x}$-$\vec{v}$ phase space. Indeed, this is the

reason why δf methods so far treat the momentum and energy conservation term $C(f_0, f_1)$ as a source term and implement it via the introduction of an additional dimension, particle weight w.

A convenient choice for the marker sources is $S_M = \nu(t)s(\vec{r})f_0\delta(w)$ and $\Omega_M = \nu(t)s(\vec{r})f_0\delta(\omega)$. This choice means that new Maxwellian markers with $w = \omega = 0$ are added in terms of rate $\nu(t)$ and spatial distribution $s(\vec{r})$. Then the weight equations are simplified to

$$\dot{w} = \frac{1-\omega}{f_0}\left[-\vec{v_d}\cdot\nabla f_0 + C(f_0, f_1)\right]. \qquad (51)$$

$$\dot{\omega} = \frac{1-\omega}{f_0}\left[-\vec{v_d}\cdot\nabla f_0 + \nu s f_0\right]. \qquad (52)$$

To test this accurate weighting scheme, we now apply it to solving Eq.(4) for ions including only ion-ion collisions. The problem considered here is the same as that in Sec. IV except an exponential density profile $n(r) \sim e^{-r^2/l^2}$ used instead of the linear density profile. In our opinion for this density profile the nonlinear weighting scheme could be ineffective since it is not easy to find an appropriate marker source S_M to implement $g = f$. The results of simulations using the previous nonlinear scheme and the present new scheme, but with the same source S_M, are compared in Fig. 4. Figure 4(a) shows that the density profile in steady state deviates far from the equilibrium. Correspondingly, the nonlinear weighting scheme fails to give the correct particle flux and energy flux, as shown in Figs. 4(b) and (c), because $g = f$ is not recognized in the simulation. While the accurate weighting scheme works for the problem effectively; it leads to the correct results with vanishing particle and energy fluxes at the whole poloidal section.

VI. SUMMARY

We presented a like-particle collision scheme for δf simulation, with excellence accuracy in conservation of particle, momentum and energy.

We demonstrated the essence of estimating the marker density g for δf method. The correct result is assured only when the assumed g for calculating weights is correctly represented by marker distribution. In the case collisions along with drift motion lead to marker diffusion through and loss from the simulation domain, this requirement, in principle, might be achieved by redistributing the markers via an appropriate source S_M. But practical implementation is difficult, even not possible.

We developed a general and accurate weighting scheme where additional weight equation is introduced to solve g directly from its kinetic equation. The new weighting scheme is more effective and can avoid implementing difficulty of previous weighting scheme in estimating the distribution function g.

This accurate δf method has been applied to the study of ion neoclassical transport due to self-collisions.

ACKNOWLEDGMENTS

One of the authors (Wang) thanks Dr. H. Saleem for his helps during the preparation of the paper. The numerical simulations were performed on SX4 super computer system of NIFS.

REFERENCES

[1] M. Kotschenruether, Bull. Am. Phys. Soc. **34**, 2107(1988).

[1] M. Kotschenruether, Proceedings of the 14th International Conference on the Numerical Simulation of Plasmas (SAIC-NRL, Annapolis, MD, 1991).

[3] A. M. Dimits and W. W. Lee, J. Comput. Phys. **107**, 309(1993).

[4] S. Parker and W. W. Lee, Phys. Fluids B **5**,

77(1993).

[5] G. Hu and J. A. Krommes, Phys. Plasmas **1**, 862(1994).

[6] Z. Lin, M. W. Tang and W. W. Lee, Phys. Plasmas **2**, 2975(1995).

[7] Z. Lin. M. W. Tang and W. W. Lee, Phys. Plasmas **4**, 1707(1997).

[8] F. L. Hinton and R. D. Hazeltine, Rev. Mod. Phys. **48**, 239(1976).

[9] A. M. Dimits and B. I. Cohen, Phys. Rev. E **49**, 709(1994).

[10] P. J. Catto and K. T. Tsang, Phys. Fluids **20**, 396(1977).

[11] X. Q. Xu and M. N. Rosenbluth, Phys. Fluids B **3**, 627(1991).

[12] Y. Chen and R. B. White. Phys. Plasmas **4**. 3591(1997).

[13] T. D. Rognlien and T. A. Cutler. Nucl. Fusion **20**. 1003(1980).

FIGURE CAPTIONS

Fig. 1 Test results of like particle collision schemes from solving Eq. (28). The plots are the time history of (a) relative energy, (c) relative momentum and (d) relative weight (or particle number). (b) is the enlarged one from (a). The lines with open circles are obtained from using the previous operator due to Lin, Tang and Lee; the lines with squares are obtained by adding $P_1 f_M$ and that with triangles are obtained by adding $(P_1 f_M + P_2 f_M)$; the lines with solid circles represent the results of improved operator with $(P_1 f_M + P_2 f_M + Q_1 f_M + Q_2 f_M)$ implemented. Time is normalized by like-particle collision time τ_{aa}.

Fig. 2 Simulation results of the solution of Eq.(5) (zero banana width limit) for ions. using the improved operator as well as the operator by Lin. Tang and Lee. The plots are time evolution of (a) particle flux (time averaging). (b) energy flux (time averaging) and (b) parallel velocity. as well as (d) distribution function in steady state (solid line represents the exact solution of Eq. (5)—shifted Maxwellian). Particle flux Γ_0 and energy flux Q_0 used for normalization are computed from using non-conservation operator C_{TP}, and parallel velocity is normalized by its theoretical value $u_{\|T}$. Time is normalized by ion collision time τ_{ii}.

Fig. 3 Simulation results from solving Eq.(4) (with finite banana width) by the nonlinear weighting scheme. Two simulations are performed with different marker sources $S_{M,A}$ and $S_{M,B}$. The plots are (a) marker density profiles. the time evolution of (b) particle flux (time averaging) and (c) energy flux (time averaging) at $r/a = 0.5$ for source B. (d) particle flux and (e) energy flux vs r/a (solid circles and open circles represent the results for source A and B respectively, and squares represent the results from using non-conservation operator C_{TP} and source B). (f) time evolution of parallel velocity at $r/a = 0.5$ and (g) parallel velocity vs r/a for source B.

Fig. 4 Simulation results from solving Eq.(4) with an equilibrium density profile $n(r) \sim e^{-r^2/l^2}$, using the nonlinear weighting scheme and new weighting scheme but with the same marker source. The plots are (a) marker density profile, (b) particle flux and (c) energy flux vs r/a.

Fig.1(a)

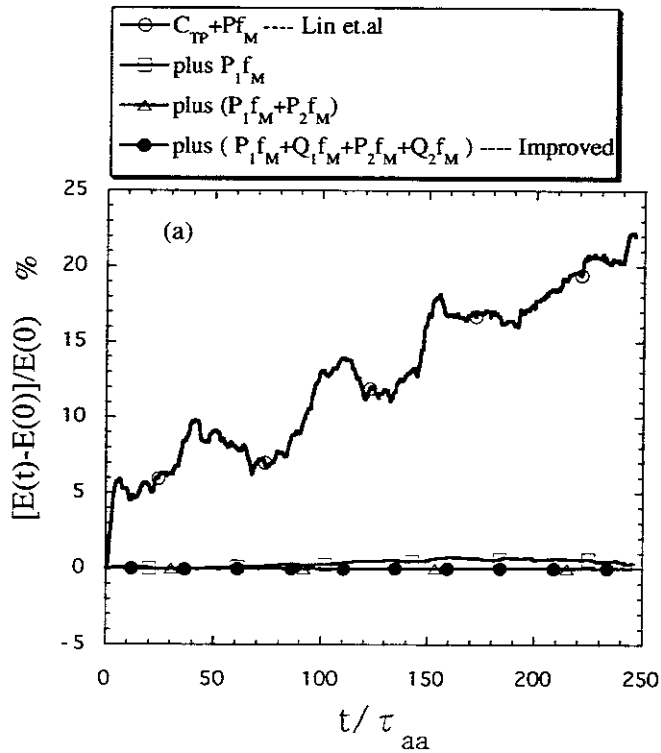
$C_{TP}+Pf_M$ ---- Lin et.al
plus P_1f_M
plus $(P_1f_M+P_2f_M)$
plus ($P_1f_M+Q_1f_M+P_2f_M+Q_2f_M$) ---- Improved
(a)
[E(t)-E(0)]/E(0) %
25
20
15
10
5
0
-5
0
50
100
150
200
250
t/ τ_{aa}

Fig. 1(b)

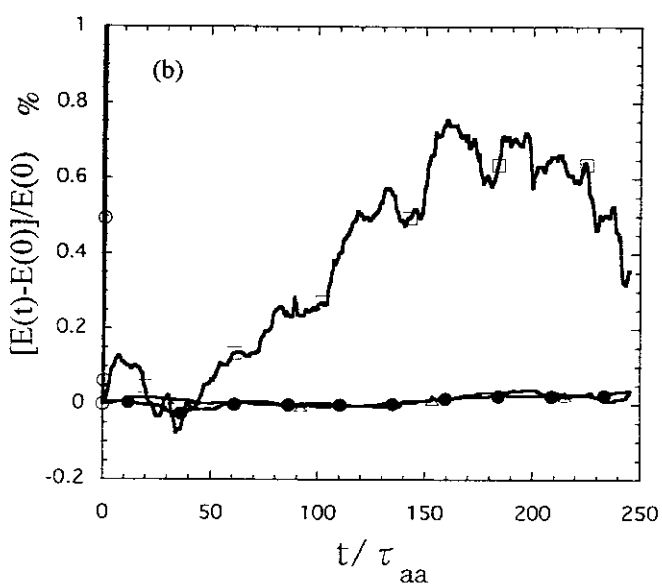
(b)
[E(t)-E(0)]/E(0) %
1
0.8
0.6
0.4
0.2
0
-0.2
0
50
100
150
200
250
t/ τ_{aa}

Fig. 1(c)

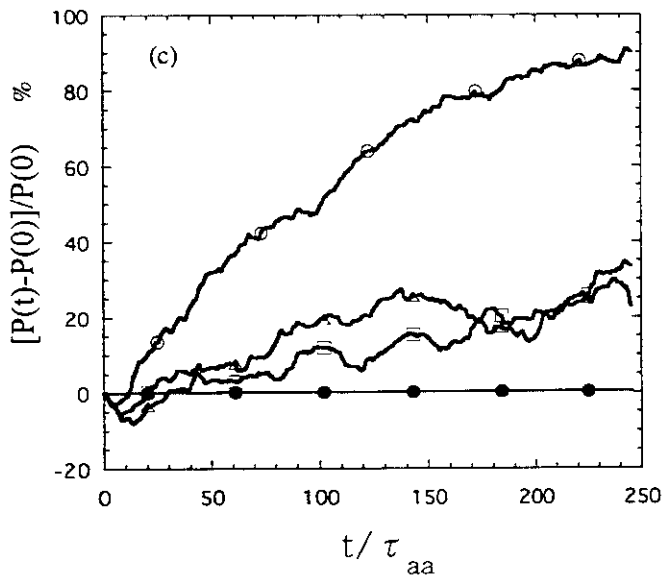
(c)
[P(t)-P(0)]/P(0) %
100
80
60
40
20
0
-20
0
50
100
150
200
250
t/ τ aa

Fig. 1(d)

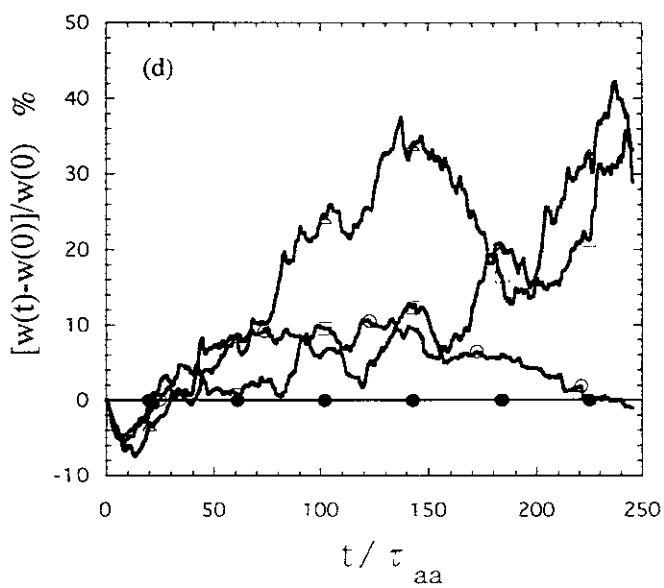
(d)
[w(t)-w(0)]/w(0) %
50
40
30
20
10
0
-10
0
50
100
150
200
250
t / τ aa

Fig. 2(a)

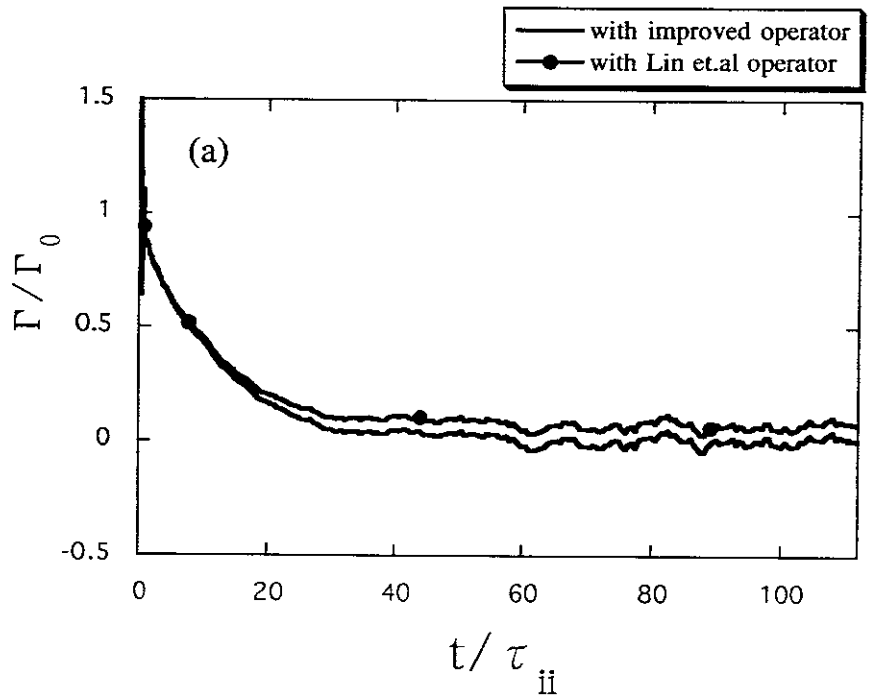
with improved operator
with Lin et.al operator
(a)
1.5
1
0.5
0
-0.5
Γ / Γ0
0
20
40
60
80
100
t / τii

Fig. 2(b)

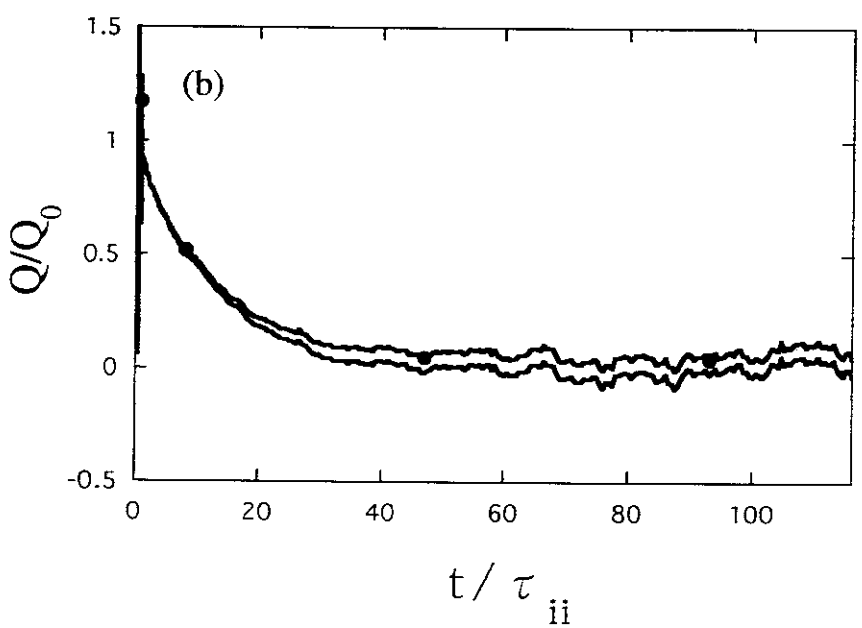
(b)
1.5
1
0.5
0
-0.5
Q/Q0
0
20
40
60
80
100
t / τii

Fig. 2(c)

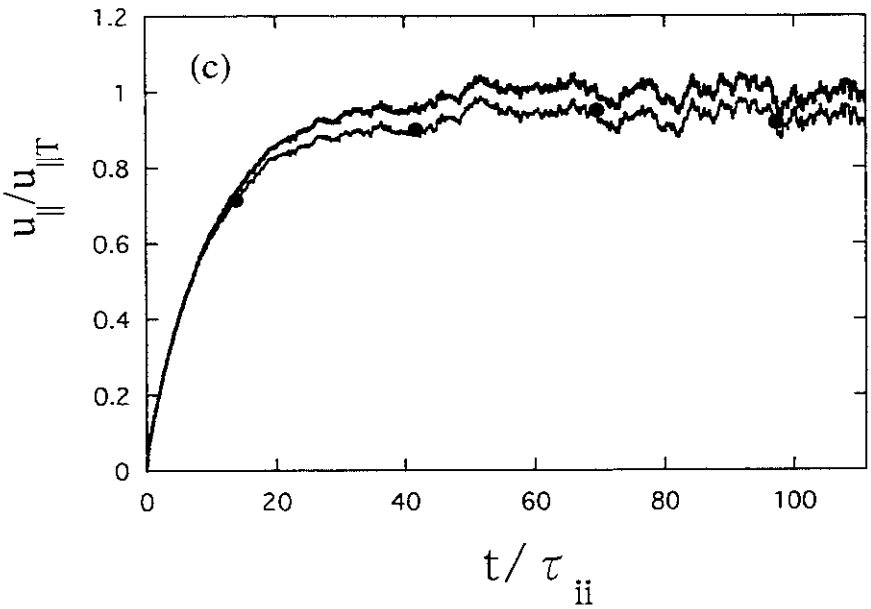
(c)
1.2
1
0.8
0.6
0.4
0.2
0
0
20
40
60
80
100
$u_{\parallel}/u_{\parallel T}$
t/τ_{ii}

Fig. 2(d)

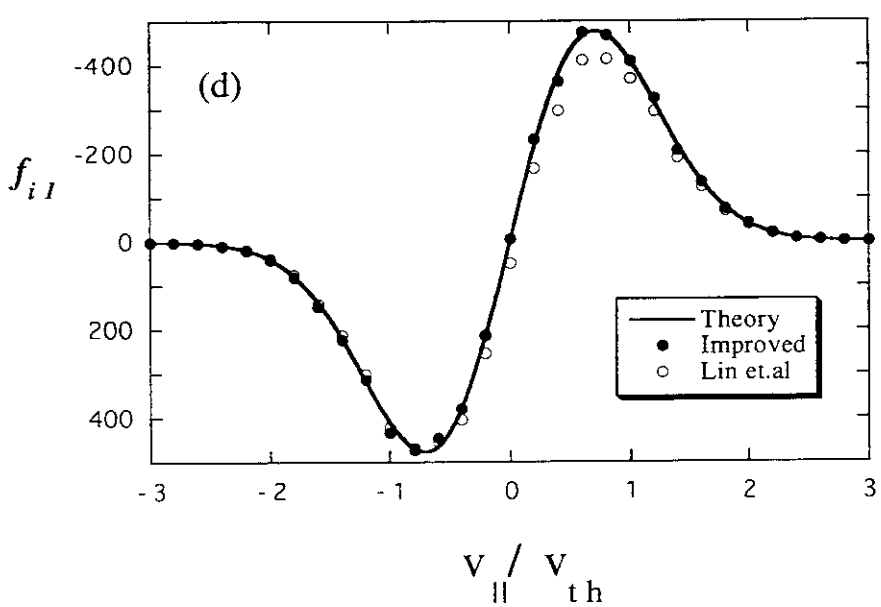
(d)
-400
-200
0
200
400
-3
-2
-1
0
1
2
3
Theory
Improved
Lin et.al
$f_{i\,I}$
$v_{\parallel}/v_{th}$

Fig. 3(a)

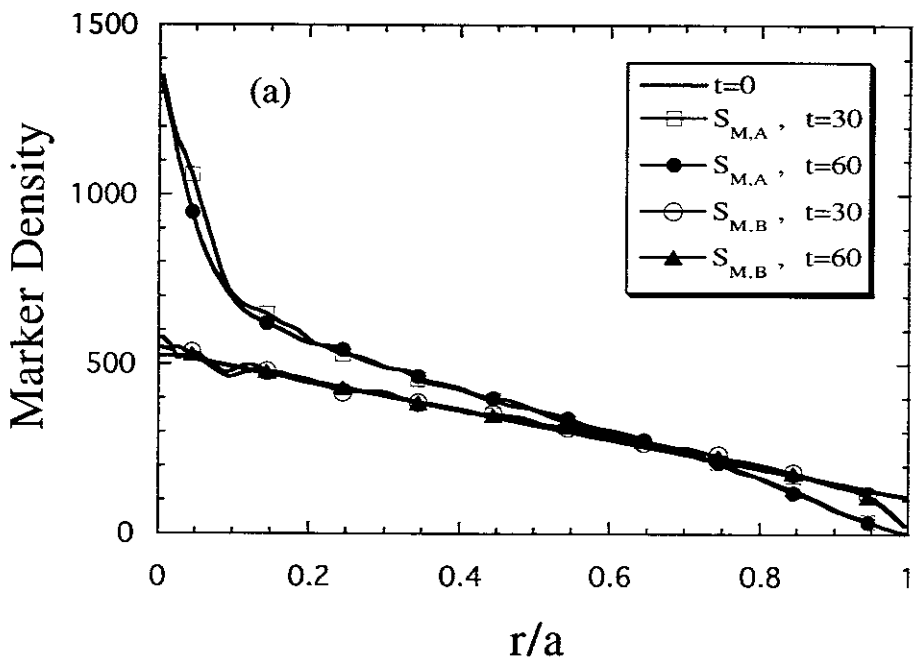
(a)
Marker Density
1500
1000
500
0
0
0.2
0.4
0.6
0.8
1
r/a
t=0
$S_{M,A}$, t=30
$S_{M,A}$, t=60
$S_{M,B}$, t=30
$S_{M,B}$, t=60

Fig. 3(b)

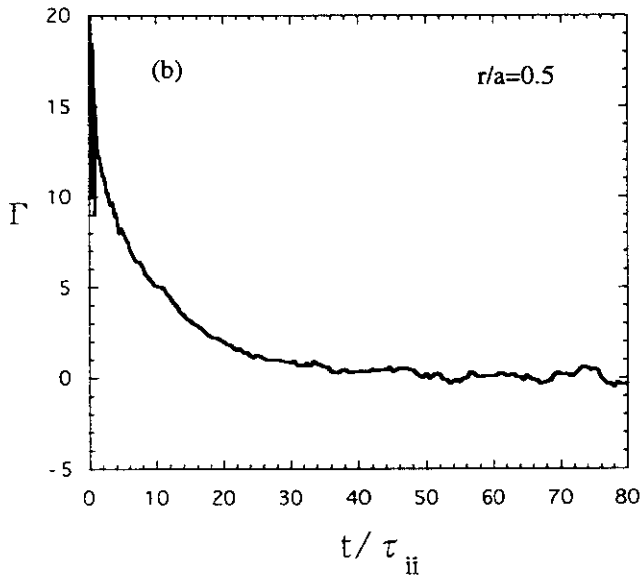
(b)
r/a=0.5
Γ
20
15
10
5
0
-5
0
10
20
30
40
50
60
70
80
t/ τ ii

Fig. 3(c)

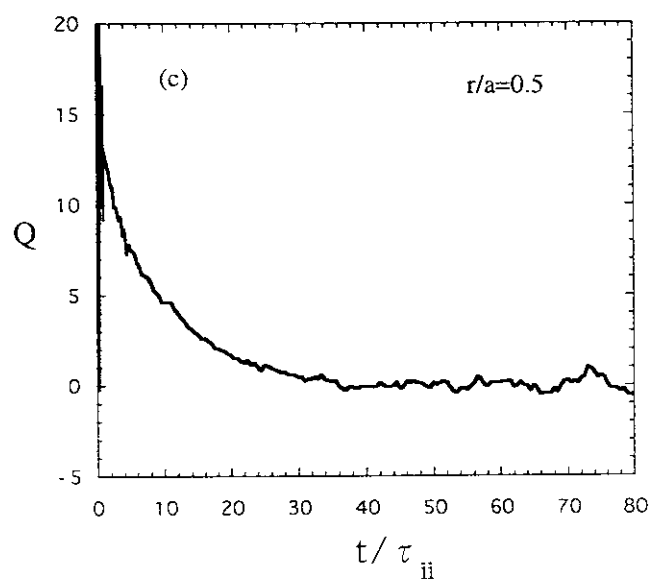
(c)
r/a=0.5
Q
20
15
10
5
0
-5
0
10
20
30
40
50
60
70
80
t/ τ ii

Fig. 3(d)

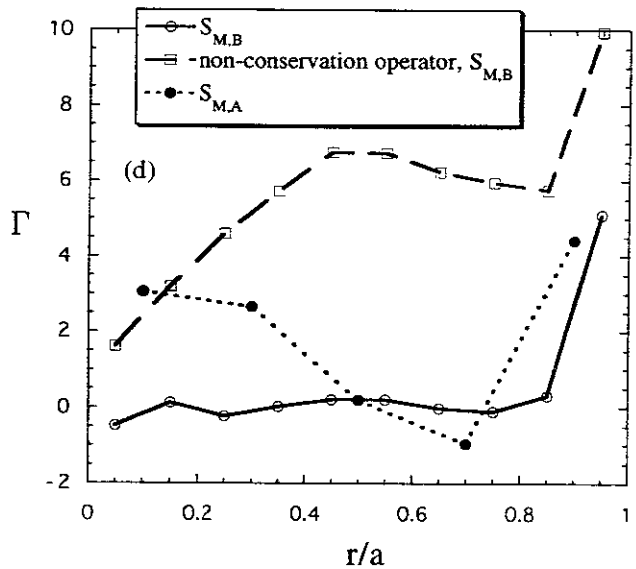
$S_{M,B}$
non-conservation operator, $S_{M,B}$
$S_{M,A}$
(d)
Γ
r/a
10
8
6
4
2
0
-2
0
0.2
0.4
0.6
0.8
1

Fig. 3(e)

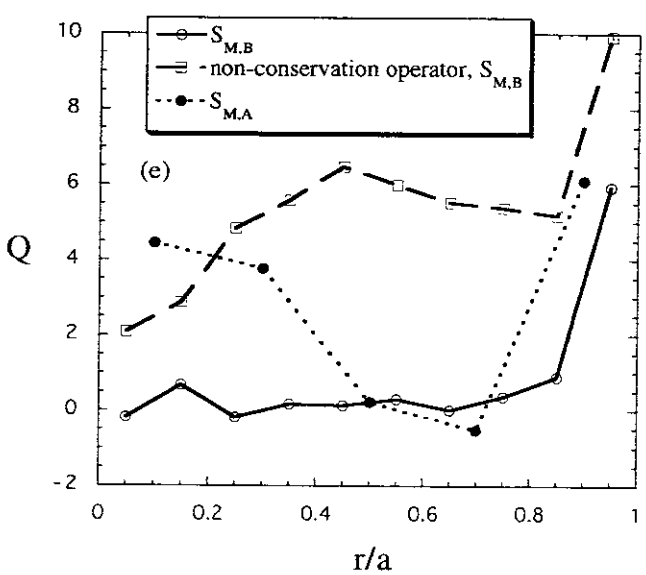
$S_{M,B}$
non-conservation operator, $S_{M,B}$
$S_{M,A}$
(e)
Q
r/a
10
8
6
4
2
0
-2
0
0.2
0.4
0.6
0.8
1

Fig. 3(f)

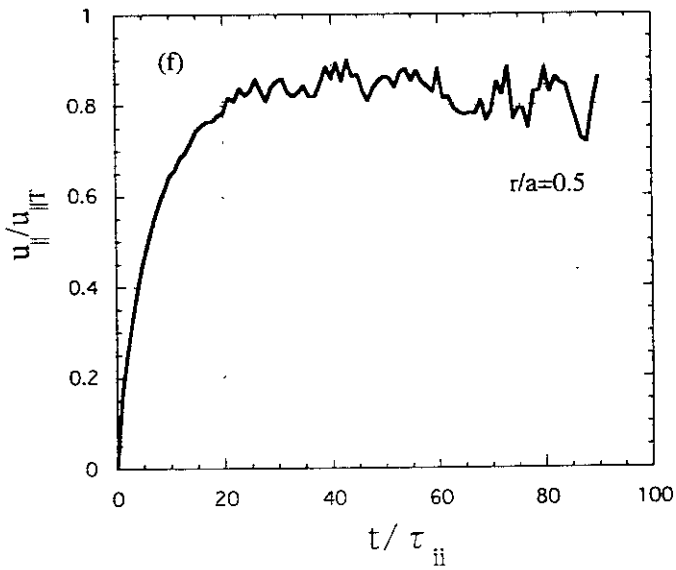
(f)
r/a=0.5
$u_{||}/u_{||r}$
t/τ_{ii}
0
0.2
0.4
0.6
0.8
1
0
20
40
60
80
100

Fig. 3(g)

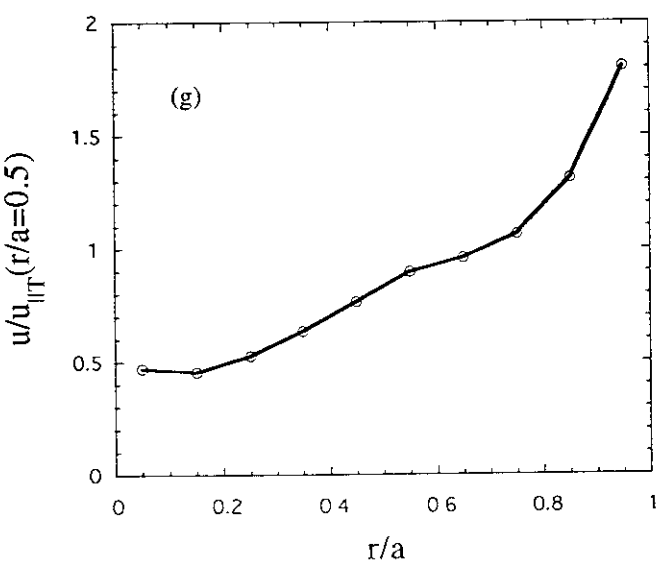
(g)
$u/u_{||r}(r/a=0.5)$
r/a
0
0.5
1
1.5
2
0
0.2
0.4
0.6
0.8
1

Fig. 4(a)

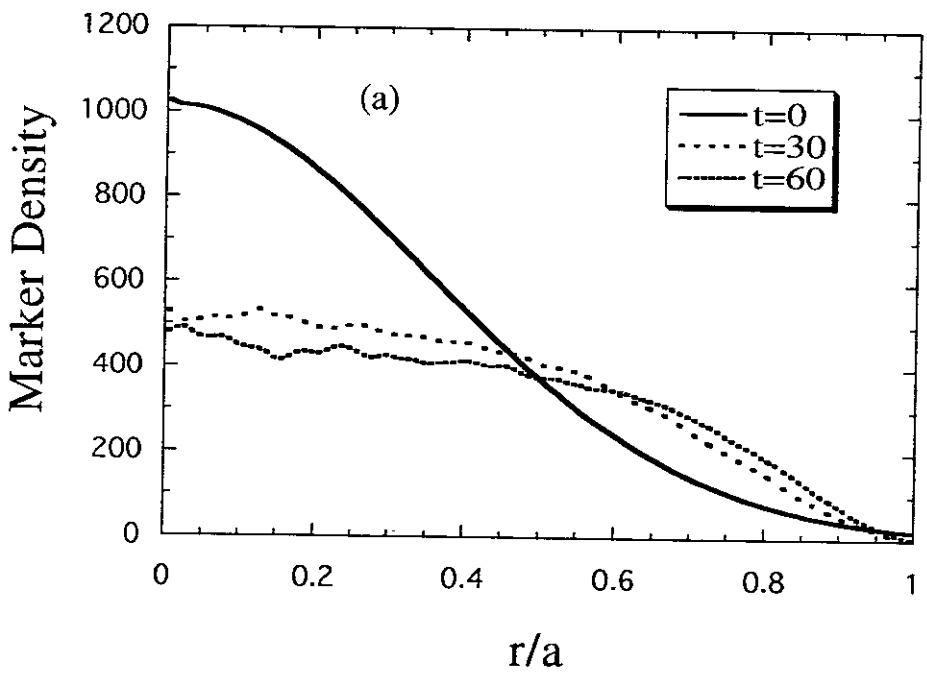
(a)
t=0
t=30
t=60
Marker Density
r/a
1200
1000
800
600
400
200
0
0
0.2
0.4
0.6
0.8
1

Fig. 4(b)

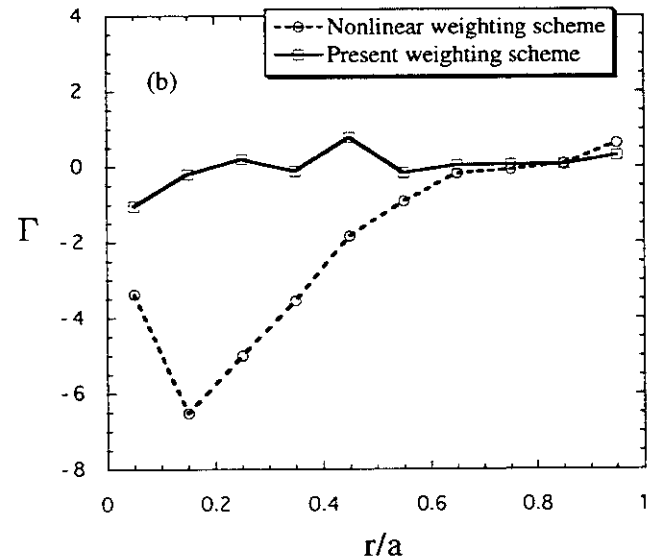
Nonlinear weighting scheme
Present weighting scheme
(b)
Γ
r/a
4
2
0
-2
-4
-6
-8
0
0.2
0.4
0.6
0.8
1

Fig. 4(c)

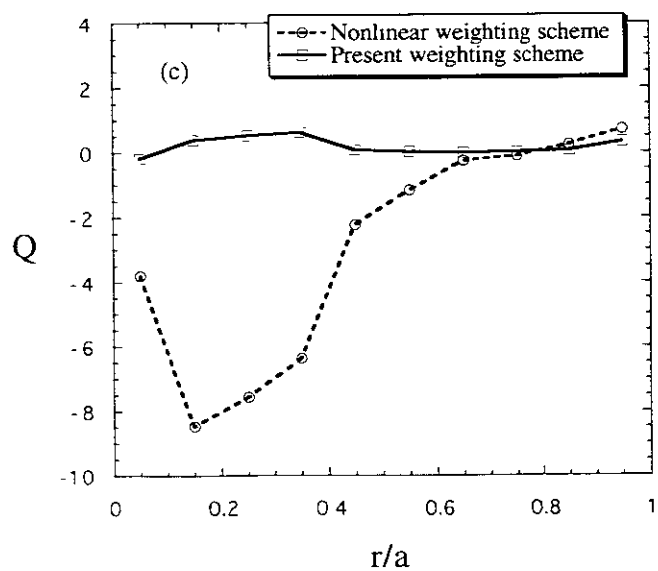
Nonlinear weighting scheme
Present weighting scheme
(c)
Q
r/a
4
2
0
-2
-4
-6
-8
-10
0
0.2
0.4
0.6
0.8
1

Recent Issues of NIFS Series

NIFS-524 T Ohkawa,
Tunneling Electron Trap; Dec. 1997

NIFS-525 K. Itoh, S.-I Itoh, M Yagi, A. Fukuyama,
Solitary Radial Electric Field Structure in Tokamak Plasmas; Dec. 1997

NIFS-526 Andrey N Lyakhov,
Alfven Instabilities in FRC Plasma, Dec. 1997

NIFS-527 J. Uramoto,
Net Current Increment of negative Muonlike Particle Produced by the Electron and Positive Ion Bunch-method; Dec. 1997

NIFS-528 Andrey N. Lyakhov,
Comments on Electrostastic Drift Instabilities in Field Reversed Configuration, Dec 1997

NIFS-529 J. Uramoto,
Pair Creation of Negative and Positive Pionlike (Muonlike) Particle by Interaction between an Electron Bunch and a Positive Ion Bunch; Dec 1997

NIFS-530 J. Uramoto,
Measuring Method of Decay Time of Negative Muonlike Particle by Beam Collector Applied RF Bias Voltage; Dec. 1997

NIFS-531 J. Uramoto,
Confirmation Method for Metal Plate Penetration of Low Energy Negative Pionlike or Muonlike Particle Beam under Positive Ions; Dec. 1997

NIFS-532 J. Uramoto,
Pair Creations of Negative and Positive Pionlike (Muonlike) Particle or K Mesonlike (Muonlike) Particle in H2 or D2 Gas Discharge in Magnetic Field; Dec. 1997

NIFS-533 S. Kawata, C Boonmee, T. Teramoto, L. Drska, J. Limpouch, R. Liska, M. Sinor,
Computer-Assisted Particle-in-Cell Code Development; Dec. 1997

NIFS-534 Y. Matsukawa, T Suda, S. Ohnuki and C. Namba,
Microstructure and Mechanical Property of Neutron Irradiated TiNi Shape Memory Alloy, Jan. 1998

NIFS-535 A. Fujisawa, H. Iguchi, H Idei, S. Kubo, K. Matsuoka, S. Okamura, K Tanaka, T Minami, S. Ohdachi, S. Morita, H Zushi, S. Lee, M. Osakabe, R. Akiyama, Y. Yoshimura, K. Toi, H. Sanuki, K. Itoh, A. Shimizu, S. Takagi, A Ejiri, C. Takahashi, M. Kojima, S. Hidekuma, K. Ida, S. Nishimura, N Inoue, R. Sakamoto, S.-I. Itoh, Y. Hamada, M. Fujiwara,
Discovery of Electric Pulsation in a Toroidal Helical Plasma; Jan. 1998

NIFS-536 Lj.R Hadzievski, M.M Skoric, M. Kono and T. Sato,
Simulation of Weak and Strong Langmuir Collapse Regimes; Jan. 1998

NIFS-537 H. Sugama, W Horton,
Nonlinear Electromagnetic Gyrokinetic Equation for Plasmas with Large Mean Flows; Feb 1998

NIFS-538 H Iguchi, T.P. Crowley, A. Fujisawa, S. Lee, K. Tanaka, T. Minami, S Nishimura, K. Ida, R. Akiyama, Y. Hamada, H., Idei. M. Isobe, M. Kojima, S. Kubo, S. Morita, S. Ohdachi, S. Okamura, M. Osakabe, K Matsuoka, C. Takahashi and K. Toi,
Space Potential Fluctuations during MHD Activities in the Compact Helical System (CHS); Feb. 1998

NIFS-539 Takashi Yabe and Yan Zhang,
Effect of Ambient Gas on Three-Dimensional Breakup in Coronet Formation Process; Feb. 1998

NIFS-540 H Nakamura, K Ikeda and S Yamaguchi,
Transport Coefficients of InSb in a Strong Magnetic Field, Feb 1998

NIFS-541 J. Uramoto,
Development of ν_μ Beam Detector and Large Area ν_μ Beam Source by H_2 Gas Discharge (I); Mar. 1998

NIFS-542 J. Uramoto,
Development of bar{ν}$_\mu$ Beam Detector and Large Area bar{ν}$_\mu$ Beam Source by H_2 Gas Discharge (II); Mar. 1998

NIFS-543 J. Uramoto,
Some Problems inside a Mass Analyzer for Pions Extracted from a H_2 Gas Discharge; Mar. 1998

NIFS-544 J. Uramoto,
Simplified ν_{μ} bar{ν}$_\mu$ Beam Detector and ν_{μ} bar{ν}$_\mu$ Beam Source by Interaction between an Electron Bunch and a Positive Ion Bunch; Mar. 1998

NIFS-545 J. Uramoto,
Various Neutrino Beams Generated by D_2 Gas Discharge; Mar.1998

NIFS-546 R. Kanno, N Nakajima, T. Hayashi and M. Okamoto,
Computational Study of Three Dimensional Equilibria with the Bootstrap Current; Mar. 1998

NIFS-547 R. Kanno, N. Nakajima and M. Okamoto,
Electron Heat Transport in a Self-Similar Structure of Magnetic Islands; Apr. 1998

NIFS-548 J.E. Rice,
Simulated Impurity Transport in LHD from MIST; May 1998

NIFS-549 M.M. Skoric, T. Sato, A.M. Maluckov and M.S. Jovanovic,
On Kinetic Complexity in a Three-Wave Interaction; June 1998

NIFS-550 S. Goto and S. Kida,
Passive Saclar Spectrum in Isotropic Turbulence: Prediction by the Lagrangian Direct-interaction Approximation; June 1998

NIFS-551 T. Kuroda, H. Sugama, R. Kanno, M. Okamoto and W. Horton,
Initial Value Problem of the Toroidal Ion Temperature Gradient Mode ; June 1998

NIFS-552 T. Mutoh, R. Kumazawa, T. Seki, F. Simpo, G. Nomura, T. Ido and T. Watari,
Steady State Tests of High Voltage Ceramic Feedthoughs and Co-Axial Transmission Line of ICRF Heating System for the Large Helical Device ; June 1998

NIFS-553 N. Noda, K. Tsuzuki, A. Sagara, N. Inoue, T. Muroga,
oronaization in Future Devices -Protecting Layer against Tritium and Energetic Neutrals-: July 1998

NIFS-554 S. Murakami and H. Saleem,
Electromagnetic Effects on Rippling Instability and Tokamak Edge Fluctuations; July 1998

NIFS-555 H. Nakamura , K. Ikeda and S. Yamaguchi,
Physical Model of Nernst Element; Aug. 1998

NIFS-556 H Okumura, S Yamaguchi, H. Nakamura, K. Ikeda and K. Sawada,
Numerical Computation of Thermoelectric and Thermomagnetic Effects, Aug. 1998

NIFS-557 Y. Takein, M. Osakabe, K. Tsumori, Y. Oka, O. Kaneko, E. Asano, T Kawamoto, R. Akiyama and M. Tanaka,
Development of a High-Current Hydrogen-Negative Ion Source for LHD-NBI System; Aug.1998

NIFS-558 M. Tanaka, A. Yu Grosberg and T. Tanaka,
Molecular Dynamics of Structure Organization of Polyampholytes;Sep. 1998

NIFS-559 R. Horiuchi, K. Nishimura and T. Watanabe,
Kinetic Stabilization of Tilt Disruption in Field-Reversed Configurations; Sep. 1998
(IAEA-CN-69/THP1/11)

NIFS-560 S. Sudo, K. Kholopenkov, K. Matsuoka, S. Okamura, C. Takahashi, R. Akiyama, A. Fujisawa, K. Ida, H. Idei, H. Iguchi, M. Isobe, S. Kado, K. Kondo, S. Kubo, H. Kuramoto, T. Minami, S. Morita, S. Nishimura, M. Osakabe, M. Sasao, B. Peterson, K. Tanaka, K. Toi and Y. Yoshimura,
Particle Transport Study with Tracer-Encapsulated Solid Pellet Injection;Oct. 1998
(IAEA-CN-69/EXP1/18)

NIFS-561 A Fujisawa, H. Iguchi, S. Lee, K Tanaka, T Minami, Y. Yoshimura, M Osakabe, K. Matsuoka, S Okamura, H Idei, S. Kubo, S. Ohdachi, S Morita, R. Akiyama, K. Toi, H. Sanuki, K. Itoh, K. Ida, A. Shimizu, S Takagi, C Takahashi, M. Kojima, S. Hidekuma, S. Nishimura, M. Isobe, A Ejiri, N Inoue, R Sakamoto, Y Hamada and M Fujiwara,
Dynamic Behavior Associated with Electric Field Transitions in CHS Heliotron/Torsatron; Oct 1998
(IAEA-CN-69/EX5/1)

NIFS-562 S Yoshikawa,
Next Generation Toroidal Devices, Oct. 1998

NIFS-563 Y Todo and T. Sato,
Kinetic-Magnetohydrodynamic Simulation Study of Fast Ions and Toroidal Alfvén Eigenmodes; Oct. 1998
(IAEA-CN-69/THP2/22)

NIFS-564 T Watari, T. Shimozuma, Y. Takeiri, R. Kumazawa, T. Mutoh, M. Sato, O. Kaneko, K. Ohkubo, S Kubo, H. Idei, Y. Oka, M. Osakabe, T. Seki, K. Tsumori, Y. Yoshimura, R. Akiyama, T. Kawamoto, S Kobayashi, F. Shimpo, Y. Takita, E. Asano, S. Itoh, G. Nomura, T. Ido, M. Hamabe, M. Fujiwara, A Iiyoshi, S Monmoto, T. Bigelow and Y.P Zhao,
Steady State Heating Technology Development for LHD; Oct. 1998
(IAEA-CN-69/FTP/21)

NIFS-565 A. Sagara, K Y. Watanabe, K. Yamazaki, O. Motojima, M Fujiwara, O Mitarai, S. Imagawa, H. Yamanishi, H Chikaraishi, A. Kohyama, H. Matsui, T Muroga, T Noda, N. Ohyabu, T. Satow, A.A Shishkin, S. Tanaka, T. Terai and T. Uda,
LHD-Type Compact Helical Reactors, Oct. 1998
(IAEA-CN-69/FTP/03(R)

NIFS-566 N. Nakajima, J. Chen, K. Ichiguchi and M. Okamoto,
Global Mode Analysis of Ideal MHD Modes in L=2 Heliotron/Torsatron Systems; Oct. 1998
(IAEA-CN-69/THP1/08)

NIFS-567 K. Ida, M Osakabe, K. Tanaka, T Minami, S Nishimura, S. Okamura, A. Fujisawa, Y. Yoshimura, S. Kubo, R. Akiyama, D.S.Darrow, H. Idei, H. Iguchi, M. Isobe, S. Kado, T. Kondo, S. Lee, K. Matsuoka, S. Morita, I Nomura, S. Ohdachi, M. Sasao, A. Shimizu, K. Tumori, S. Takayama, M. Takechi, S. Takagi, C Takahashi, K. Toi and T Watari,
Transition from L Mode to High Ion Temperature Mode in CHS Heliotron/Torsatron Plasmas; Oct 1998
(IAEA-CN-69/EX2/2)

NIFS-568 S. Okamura, K. Matsuoka, R. Akiyama, D.S. Darrow, A. Ejiri, A Fujisawa, M Fujiwara, M. Goto, K. Ida H. Idei, H. Iguchi, N. Inoue, M. Isobe, K. Itoh, S. Kado, K. Khlopenkov, T. Kondo, S. Kubo, A Lazaros, S. Lee, G. Matsunaga, T. Minami, S Morita, S. Murakami, N Nakajima, N. Nikai, S. Nishimura, I. Nomura, S. Ohdachi, K. Ohkuni, M. Osakabe, R. Pavlichenko, B. Peterson, R. Sakamoto, H. Sanuki, M. Sasao, A. Shimizu, Y. Shirai, S. Sudo, S. Takagi, C. Takahashi, S. Takayama, M. Takechi, K. Tanaka, K Toi, K. Yamazaki, Y. Yoshimura and T Watari,
Confinement Physics Study in a Small Low-Aspect-Ratio Helical Device CHS; Oct 1998
(IAEA-CN-69/OV4/5)

NIFS-569 M.M. Skoric, T. Sato, A. Maluckov, M.S. Jovanovic,
Micro- and Macro-scale Self-organization in a Dissipative Plasma, Oct 1998

NIFS-570 T Hayashi, N. Mizuguchi, T-H Watanabe, T. Sato and the Complexity Simulation Group,
Nonlinear Simulations of Internal Reconnection Event in Spherical Tokamak, Oct 1998
(IAEA-CN-69/TH3/3)

NIFS-571 A. Iiyoshi, A. Komori, A Ejiri, M. Emoto, H. Funaba, M. Goto, K Ida, H. Idei, S Inagaki, S. Kado, O Kaneko, K. Kawahata, S. Kubo, R. Kumazawa, S. Masuzaki, T. Minami, J. Miyazawa, T. Morisaki, S Morita, S. Murakami, S. Muto, T. Muto, Y. Nagayama, Y. Nakamura, H. Nakanishi, K Narihara, K. Nishimura, N. Noda, T Kobuchi, S. Ohdachi, N. Ohyabu, Y. Oka, M. Osakabe, T. Ozaki, B.J Peterson, A Sagara, S. Sakakibara, R. Sakamoto, H. Sasao, M Sasao, K. Sato, M. Sato, T. Seki, T. Shimozuma, M. Shoji, H. Suzuki, Y Takeiri, K. Tanaka, K. Toi, T. Tokuzawa, K. Tsumori, I. Yamada, H. Yamada, S. Yamaguchi, M. Yokoyama, K.Y.Watanabe, T. Watari, R. Akiyama, H. Chikaraishi, K. Haba, S Hamaguchi, S. Iima, S. Imagawa, N. Inoue, K Iwamoto, S. Kitagawa, Y. Kubota, J. Kodaira, R Maekawa, T. Mito. T Nagasaka, A Nishimura, Y. Takita, C. Takahashi, K. Takahata, K. Yamauchi, H. Tamura, T. Tsuzuki, S. Yamada, N. Yanagi, H. Yonezu, Y. Hamada, K. Matsuoka, K. Murai, K. Ohkubo, I. Ohtake, M. Okamoto, S. Sato, T Satow, S Sudo, S. Tanahashi, K. Yamazaki, M. Fujiwara and O. Motojima,
An Overview of the Large Helical Device Project; Oct. 1998
(IAEA-CN-69/OV1/4)

NIFS-572 M Fujiwara, H. Yamada, A. Ejiri, M. Emoto, H. Funaba, M Goto, K Ida, H Idei, S. Inagaki, S Kado, O Kaneko, K. Kawahata, A. Komori, S. Kubo, R. Kumazawa, S Masuzaki, T. Minami, J. Miyazawa, T Morisaki, S. Morita, S. Murakami, S. Muto, T Muto, Y. Nagayama, Y. Nakamura, H Nakanishi, K. Narihara, K. Nishimura, N Noda, T. Kobuchi, S. Ohdachi, N. Ohyabu, Y. Oka, M. Osakabe, T. Ozaki, B J Peterson, A. Sagara, S Sakakibara, R Sakamoto, H Sasao, M Sasao, K. Sato, M. Sato, T Seki, T. Shimozuma, M. Shoji, H. Sazuki, Y Takeiri, K Tanaka, K Toi, T Tokuzawa, K Tsumori, I. Yamada, S. Yamaguchi, M. Yokoyama, K.Y Watanabe, T. Watari, R. Akiyama, H Chikaraishi, K. Haba, S. Hamaguchi, M. Iima, S Imagawa, N. Inoue, K. Iwamoto, S. Kitagawa, Y. Kubota, J. Kodaira, R. Maekawa, T. Mito, T. Nagasaka, A Nishimura, Y. Takita, C. Takahashi, K. Takahata, K Yamauchi, H. Tamura, T. Tsuzuki, S Yamada, N Yanagi, H Yonezu, Y. Hamada, K. Matsuoka, K. Murai, K Ohkubo, I. Ohtake, M. Okamoto, S Sato, T Satow, S Sudo, S Tanahashi, K. Yamazaki, O. Motojima and A. Iiyoshi,
Plasma Confinement Studies in LHD; Oct 1998
(IAEA-CN-69/EX2/3)

NIFS-573 O. Motojima, K. Akaishi, H. Chikaraishi, H. Funaba, S. Hamaguchi, S. Imagawa, S. Inagaki, N. Inoue, A. Iwamoto, S. Kitagawa, A. Komori, Y. Kubota, R. Maekawa, S. Masuzaki, T. Mito, J. Miyazawa, T. Morisaki, T. Muroga, T. Nagasaka, Y Nakmura, A. Nishimura, K. Nishimura, N. Noda, N. Ohyabu, S. Sagara, S. Sakakibara, R. Sakamoto, S. Satoh, T. Satow, M Shoji, H. Suzuki, K. Takahata, H. Tamura, K. Watanabe, H. Yamada, S. Yamada, S. Yamaguchi, K. Yamazaki, N. Yanagi, T. Baba, H. Hayashi, M. Iima, T. Inoue, S. Kato, T. Kato, T. Kondo, S. Moriuchi, H. Ogawa, I. Ohtake, K. Ooba, H. Sekiguchi, N. Suzuki, S. Takami, Y. Taniguchi, T. Tsuzuki, N. Yamamoto, K. Yasui, H. Yonezu, M. Fujiwara and A. Iiyoshi,
Progress Summary of LHD Engineering Design and Construction; Oct. 1998
(IAEA-CN-69/FT2/1)

NIFS-574 K. Toi, M. Takechi, S. Takagi, G. Matsunaga, M. Isobe, T. Kondo, M. Sasao, D.S. Darrow, K. Ohkuni, S. Ohdachi, R. Akiyama A. Fujisawa, M. Gotoh, H. Idei, K. Ida, H. Iguchi, S. Kado, M. Kojima, S. Kubo, S. Lee, K. Matsuoka, T. Minami, S. Morita, N. Nikai, S. Nishimura, S. Okamura, M. Osakabe, A. Shimizu, Y. Shirai, C. Takahashi, K. Tanaka, T. Watari and Y. Yoshimura,
Global MHD Modes Excited by Energetic Ions in Heliotron/Torsatron Plasmas;Oct. 1998
(IAEA-CN-69/EXP1/19)

NIFS-575 Y. Hamada, A. Nishizawa, Y Kawasumi, A. Fujisawa, M. Kojima, K. Narihara, K. Ida, A. Ejiri, S Ohdachi, K. Kawahata, K. Toi, K. Sato, T. Seki, H. Iguchi, K Adachi, S. Hidekuma, S.Hirokura, K. Iwasaki, T. Ido, R Kumazawa, H Kuramoto, T Minami, I.. Nomura, M. Sasao, K.N. Sato, T. Tsuzuki, I. Yamada and T. Watari,
Potential Turbulence in Tokamak Plasmas;Oct. 1998
(IAEA-CN-69/EXP2/14)

NIFS-576 S. Murakami, U. Gasparino, H. Idei, S. Kubo, H. Maassberg, N. Marushchenko, N. Nakajima, M. Romé and M. Okamoto,
5D Simulation Study of Suprathermal Electron Transport in Non-Axisymmetric Plasmas;Oct. 1998
(IAEA-CN-69/THP1/01)

NIFS-577 S. Fujiwara and T. Sato,
Molecular Dynamics Simulation of Structure Formation of Short Chain Molecules; Nov. 1998

NIFS-578 T. Yamagishi,
Eigenfunctions for Vlasov Equation in Multi-species Plasmas Nov. 1998

NIFS-579 M. Tanaka, A. Yu Grosberg and T. Tanaka,
Molecular Dynamics of Strongly-Coupled Multichain Coulomb Polymers in Pure and Salt Aqueous Solutions;Nov. 1998

NIFS-580 J. Chen, N. Nakajima and M. Okamoto,
Global Mode Analysis of Ideal MHD Modes in a Heliotron/Torsatron System: I. Mercier-unstable Equilibria;Dec. 1998

NIFS-581 M. Tanaka, A. Yu Grosberg and T. Tanaka,
Comparison of Multichain Coulomb Polymers in Isolated and Periodic Systems: Molecular Dynamics Study; Jan. 1999

NIFS-582 V.S. Chan and S. Murakami,
Self-Consistent Electric Field Effect on Electron Transport of ECH Plasmas; Feb. 1999

NIFS-583 M. Yokoyama, N. Nakajima, M. Okamoto, Y. Nakamura and M. Wakatani,
Roles of Bumpy Field on Collisionless Particle Confinement in Helical-Axis Heliotrons;Feb. 1999

NIFS-584 T.-H. Watanabe, T. Hayashi, T. Sato, M. Yamada and H. Ji,
Modeling of Magnetic Island Formation in Magnetic Reconnection Experiment;Feb. 1999

NIFS-585 R. Kumazawa, T. Mutoh, T. Seki, F. Shinpo, G. Nomura, T. Ido, T. Watari, Jean-Marie Noterdaeme and Yangping Zhao,
Liquid Stub Tuner for Ion Cyclotron Heating, Mar. 1999

NIFS-586 A. Sagara, M. Iima, S. Inagaki, N. Inoue, H. Suzuki, K. Tsuzuki, S. Masuzaki, J. Miyazawa, S. Morita, Y. Nakamura, N. Noda, B. Peterson, S. Sakakibara, T. Shimozuma, H. Yamada, K. Akaishi, H. Chikaraishi, H. Funaba, O Kaneko, K. Kawahata, A. Komori, N. Ohyabu, O. Motojima, LHD Exp Group 1, LHD Exp. Group 2,
Wall Conditioning at the Starting Phase of LHD;Mar. 1999

NIFS-587 T. Nakamura and T. Yabe,
Cubic Interpolated Propagation Scheme for Solving the Hyper-Dimensional Vlasov-Poisson Equation in Phase Space;Mar. 1999

NIFS-588 W.X. Wang, N. Nakajima, S. Murakami and M. Okamoto,
An Accurate δf Method for Neoclassical Transport Calculation;Mar. 1999